

# HidePrint: Hiding the Radio Fingerprint via Random Noise

Gabriele Oligeri

*College of Science and Engineering, Hamad Bin Khalifa University, Doha, Qatar.*

Savio Sciancalepore

*Eindhoven University of Technology*

## Abstract

Radio Frequency Fingerprinting (RFF) techniques allow a receiver to authenticate a transmitter by analyzing the physical layer of the radio spectrum. Although the vast majority of scientific contributions focus on improving the performance of RFF considering different parameters and scenarios, in this work, we consider RFF as an attack vector to identify and track a target device.

We propose, implement, and evaluate *HidePrint*, a solution to prevent tracking through RFF without affecting the quality of the communication link between the transmitter and the receiver. *HidePrint* hides the transmitter's fingerprint against an illegitimate eavesdropper by injecting controlled noise in the transmitted signal. We evaluate our solution against state-of-the-art image-based RFF techniques considering different adversarial models, different communication links (wired and wireless), and different configurations. Our results show that the injection of a Gaussian noise pattern with a standard deviation of (at least) 0.02 prevents device fingerprinting in all the considered scenarios, thus making the performance of the identification process indistinguishable from the random guess while affecting the Signal-to-Noise Ratio (SNR) of the received signal by only 0.1 dB. Moreover, we introduce the *selective radio fingerprint disclosure*, a new technique that allows the transmitter to disclose the radio fingerprint to only a subset of intended receivers. This technique allows the transmitter to regain anonymity, thus preventing identification and tracking while allowing authorized receivers to authenticate the transmitter without affecting the quality of the transmitted signal.

## 1 Introduction

Radio Frequency Fingerprinting (RFF) is a popular technique used to differentiate and identify Radio Frequency (RF)-enabled devices by taking advantage of the unique characteristics inherent in the RF emissions [1]. These unique characteristics come from the hardware of the device, and in particular,

by the small differences featured by the hardware components during the manufacturing process. Such differences lead to the main idea that two electronic devices that are exactly alike do not exist because of differences in oscillators, amplifiers, and built-in antennas. Since these differences are reflected in the over-the-air signal, a receiver can extract them through the analysis of the received signals and leverage them to uniquely identify the transmitter [2]. A strict requirement for all RFF systems is the ability to collect information from the physical layer of the communication link [3]. Such features persist on the receiver side up to the conversion between symbols to bits, making the availability of such information a requirement for RFF. At the physical layer, the baseband signal can be represented by In-Phase - Quadrature (IQ) samples representing the in-phase (I) and quadrature (Q) components, used to carry the information associated with the transmitted bit string and some additional information such as noise, attenuation, Doppler shift, and finally, the radio fingerprint [4].

RFF features several key advantages compared to traditional cryptographic solutions. RFF is crypto less, i.e., it requires no implementation of cryptographic techniques, and, most importantly, it requires no key distribution, thus solving by design the challenges related to joining and leaving entities from the network. Moreover, RFF does not require any intervention on the transmitter side. The transmitter is authenticated by the information (not so) hidden in its transmitted signal. In contrast, RFF requires a receiver capable of collecting information from the physical layer and a Deep Learning (DL) model. The receiver should train a neural network with legitimate signals (IQ samples) in order to challenge it in the subsequent phase, with a test set (of IQ samples) to assess either the presence or the absence of the transmitter(s) [5].

Scientific literature in the latest years mostly focused on maximizing the performance of RFF techniques while addressing several real-world challenges, such as robustness to multipath fading [6], time-varying distortions [7], reliability over time [8], and mobility of the transmitter [9], to name a few. As a result, RFF solutions today are becoming increasingly effective for successfully classifying and authen-

ticating the transmitter, making RFF a real candidate to implement authentication at the physical layer while mitigating the common challenges of key distribution in dense networks and implementation in resource-constrained devices. While a ready-to-market RFF solution is not yet available, the accuracy of the proposed techniques is increasing for the most diverse scenarios and applications [2].

In this work, we propose a different perspective on RFF, exploring the possibility of adopting RFF by a malicious third party to detect and track the presence of a device in the radio spectrum. Indeed, an adversary could train a neural network model on signals generated by a specific (pool of) device(s) and then leverage such a model to detect the presence of the transmitter in the radio spectrum—making useless any anonymization technique implemented by the higher communications layers, e.g., MAC address anonymization. Malicious detection and tracking of devices pose significant challenges to people’s privacy, enabling mass and targeted surveillance. To provide an example, a practical use case might involve tracking when and where a device appears in the radio spectrum to infer a person’s daily routine, places of interest, and social interactions. Research on RFF-based attacks is relatively scarce in the literature and is mostly qualitative. Although pioneering contributions consider RFF techniques based on Channel State Information (CSI) fingerprinting [10, 11], a few contributions explored the usage of Adversarial Machine Learning (AML) techniques to generate perturbations in the transmitted signals thwarting RFF while keeping the communication quality acceptable [12], [13], [14], and [15]. However, such works either focus on pure data analysis without considering the technical challenges of data manipulation and wireless transmission or use simplistic RFF models, being far-away from real-world deployments. As a result, no contributions investigated the potential of intentionally altering the radio fingerprint to prevent the tracking of the transmitter while allowing authorized receivers to authenticate it without affecting the quality of the communication link.

**Research Questions.** In this work, we formulate the problem mentioned above through two main research questions.

*RQ1: Is it possible to prevent a malicious adversary from successfully using RFF to identify and track a (pool of) device(s)?*

*RQ2: Is it possible to design a selective radio fingerprint disclosure technique?*

Since RFF does not require shared secrets, the legitimate and malicious receivers leverage the same information. Thus, a solution preventing RFF-based attacks by an adversary (RQ1) will affect the ability of a legitimate device to authenticate the transmitter(s), thus yielding to our second research question (RQ2). Selective radio fingerprint disclosure could allow a designated set of (legitimate) receivers to perform RFF while excluding the other (malicious) ones.

**Contribution.** This work provides manifold contributions to the RFF research domain, as listed below.

- We design, implement, evaluate, and test two RFF-based attacks in different scenarios, considering both an (ideal) wired and a (real) wireless communication link.
- We consider two main adversary models as a function of the ability of the adversary to collect data from either a target device or the complete pool of devices.
- We consider an adversary capable of collecting data for RFF both before and after anonymization, so updating at runtime the RFF models to de-anonymize the transmitters.
- We provide the theoretical framework, description, real implementation, and evaluation of *HidePrint*, a solution to prevent unauthorized device fingerprinting.
- Inspired by *HidePrint*, we propose a technique enabling selective radio fingerprint disclosure, thus allowing (only) a selected subset of (legitimate) receivers to perform RFF while excluding the malicious ones.

**Paper organization.** The paper is organized as follows. Sect. 2 reviews related work about RFF, Sect. 3 introduces the adversary models and scenario assumptions used in our paper, Sect. 4 introduces the theoretical framework and rationale behind our solution, Sect. 5 provides the details of our measurement campaign and the considered hardware and software setup, Sect. 6 introduces our data pre-processing methodologies and DL techniques, Sect. 7 discusses the performance of our solution in both the wired and wireless scenarios, Sect. 8 evaluates our solution while considering competing RFF techniques, Sect. 9 presents the concept of selective radio fingerprint disclosure, Sect. 10 discusses the main results and limitations of our solution, and finally, Sect. 11 concludes the paper and outlines future work.

## 2 Related Work

RFF received a lot of attention in recent years as a technique to effectively authenticate the transmitter device [1], [2].

Early research on RFF investigated the usage of specific radio signal imperfections to identify transmitters and reject radio spoofing attacks, e.g., IQ imbalance, phase shift, and Carrier Frequency Offset (CFO), mostly using Machine Learning (ML) models [17], [18], [19]. With the diffusion of DL, research on RFF shifted towards using raw physical-layer signals, i.e., IQ samples, due to the enhanced capability of such algorithms to recognize patterns hidden in the noise [1]. Most of the solutions proposed until a few years ago leveraged raw IQ samples directly as input to various DL classifiers, e.g., Convolutional Neural Networks (CNNs) [20], Long Short-Term Memorys (LSTMs) [21], and Autoencoders (AEs) [9], to name a few. On the one hand, such solutions are characterized by outstanding classification and authentication performance, reaching accuracy values very close to perfect discrim-

Ref.	Protection against RFF	RFF Technique	Protection Strategy	No External Devices	Evaluation Strategy	Selective Radio Fingerprint Disclosure
[10]	✗	CSI-based	Phase Correction	✗	Real-world tests	✗
[11]	✓	CSI-based	Random Phase Correction	✓	Real-world tests	✗
[12]	✗	Image-based	AML	✓	Simulations	✗
[13]	✗	Raw IQ	AML	✓	Simulations	✗
[14]	✗	Raw IQ	AML	✓	Simulations	✗
[15]	✓	Raw IQ	AML	✓	Real-world tests	✗
[16]	✓	Image-based	Friendly Jamming	✗	Real-world tests	✗
<b>This Paper</b>	✓	Image-based	Random Noise	✓	Real-world tests	✓

Table 1: Qualitative comparison of scientific contributions focusing on RFF disruption.

ination [3]. On the other hand, recent research showed that the models created through these approaches are very unstable, being significantly affected by any source of noise, introduced, e.g., by the warm-up of the radio [22], hardware reset of the radio [8], temperature changes in the environment [23] [24], fluctuations in channel conditions, and firmware reload [25]. In this context, image-based RFF techniques have emerged as a branch of RFF characterized by enhanced flexibility and portability across different real-world scenarios and configurations. Recent literature has shown that pre-processing (and converting) raw IQ samples into images leads to the creation of DL-based models robust to AML [12], restart of the radios [8], and firmware reload [25], to name a few. Image-based RFF techniques have also been used beyond device identification, e.g., for distinguishing between communication channels, i.e., channel fingerprinting [26, 27], and jamming detection [28, 29]

Only a few works in the literature considered RFF as an attack and, thus, investigated how to protect a device from unconditionally disclosing the radio fingerprint to malicious parties. An early attempt in this direction is the contribution by Abanto et al. [11], showing that the injection of random phase corrections into the signal emitted by the devices can reduce the accuracy of RFF systems using CSI to authenticate a device. The RFF algorithm proposed in their paper only considers CFO and phase shift estimation, while DL-based solutions are not considered. Also, the pioneering contribution by Danev et al. in [10] considers CSI-based RFF and experiments with impersonation attacks via powerful signal generators. More recently, contributions such as the ones by Papangelo et al. [12], Sun et al. [14], and Liu et al. [13] investigated the effectiveness of AML to disrupt the correct operation of RFF. The only recent work considering the usage of adversarial techniques to conceal radio fingerprints is the preliminary work by Lu et al. in [15], providing an early solution to anonymization against RFF. The authors propose to generate a perturbation signal  $\delta$  calculated according to a predefined strategy that matches the decision algorithm taken

by the classifier. The adopted CNN network, designed from scratch, uses raw IQ samples, sharing the same limitations described above. Moreover, the authors use a limited set of devices (five) of different brands, easing the design of the RFF model and the following anonymization task, and use higher-order modulation schemes, being increasingly sensitive to even low-power noise. An alternative approach is the one proposed by Irfan et al. [16], using an external device (jammer) synchronized with the legitimate pool of devices to protect against RFF. Although effective, such an approach requires an external device, making the design of the solution more complex and enlarging the resulting threat surface.

Thus, as summarized in Tab. 1, no work in the literature investigated the ability to protect from malicious RFF while considering various adversary models, characterized by increasing knowledge of the RFF model of the target device(s), and state-of-the-art image-based RFF techniques, while avoiding to resort to additional devices. Moreover, there is currently no technique providing selective radio fingerprint disclosure, i.e., allowing the disclosure of the radio fingerprint only to selected receivers. We address this gap in the remainder of this paper.

### 3 Scenario and Adversarial model

Our scenario is constituted by a pool of ten (10) transmitters that aim to remain anonymous while communicating. Current state-of-the-art techniques already allow to enforce anonymity at higher layers of the ISO OSI communication stack, e.g., at the network layer via VPN and at the MAC layer via MAC randomization, while our scenario specifically considers anonymity against physical layer identification. Without loss of generality, we consider the usage of the Binary Phase Shift Keying (BPSK) modulation scheme. Many modern communication technologies currently use BPSK, including IEEE 802.15.4 (Zigbee, Thread), IEEE 802.11 (WiFi), and many satellite communication systems (e.g., IRIDIUM) due to its relevant robustness to noise introduced by the wire-

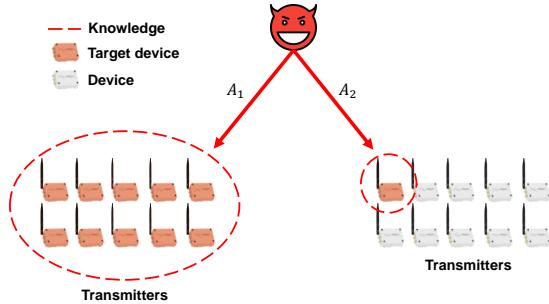


Figure 1: Adversary model. We consider two realistic assumptions: (i) the adversary owns a model containing features from all the devices in the pool ( $\mathcal{A}_1$ ) and wants to de-anonymize any of the devices in the pool, and (ii) the adversary owns a model containing features from one only device from the pool ( $\mathcal{A}_2$ ) and wants to detect its presence in the radio spectrum.

less channel [30]. Moreover, we consider an adversary able to deploy state-of-the-art image-based RFF techniques to identify and (potentially) track devices in the radio spectrum. We recall that, as discussed in Sec. 2, image-based RFF models typically outperform other solutions thanks to their enhanced robustness to noise and flexibility to real-world phenomena. Figure 1 shows our adversary model based on two different assumptions related to its apriori knowledge.

**Adversary 1 ( $\mathcal{A}_1$ ).** The adversary collects data from all devices in the pool of the transmitters, with the objective of identifying their presence in the communication link, so deanonymizing them. This objective can be formulated as a classical multiclass classification problem, where the adversary collects physical layer information from the 10 transmitters in the pool, trains a model with 10 classes (one for each transmitter), and then aims at maximizing its chances to deanonymize the transmitters (i.e., classifying them with an accuracy higher than the random guess, equal to 0.1).

**Adversary 2 ( $\mathcal{A}_2$ ).** The adversary focuses the attack on a target device, thus collecting from the physical layer of the communication link the data related to a specific transmitter. Such data is used for training a DL model to be used to detect the presence of such specific transmitter in the wild. In the remainder of this work, we address this challenge as a one-class classification problem, thus considering *autoencoders* as our identification tool.

## 4 Rationale of our Solution

Let  $I(t)$  and  $Q(t)$  be the in-phase and quadrature components (IQ components) of the baseband signal. The associated pass-band transmitted signal can be expressed as per Eq. 1:

$$x(t) = I(t) \cos(\omega_c t) + Q(t) \sin(\omega_c t), \quad (1)$$

where  $\omega_c = 2\pi f_c$  and  $f_c$  is the signal carrier. Equation 1 can be rewritten as Eq. 2:

$$x(t) = \alpha(t) \cos(\omega_c t + \phi(t)), \quad (2)$$

where  $\alpha(t) = \sqrt{I(t)^2 + Q(t)^2}$  and  $\phi(t) = \tan^{-1} \frac{Q(t)}{I(t)}$  are the amplitude and phase associated with the in-phase ( $I(t)$ ) and quadrature ( $Q(t)$ ) components of the baseband signal, respectively. We consider the BPSK modulation scheme, and therefore, we can recover the baseband signal  $r(t)$  from  $x(t)$  as:

$$\begin{aligned} r(t) &= x(t) \cdot \cos(\omega_c t) \\ &= \alpha(t) \cos(\omega_c t + \phi(t)) \cos(\omega_c t) \\ &= \frac{1}{2} \alpha(t) \cos(\phi(t)), \end{aligned} \quad (3)$$

where we have applied low-pass filtering to remove the component at frequency  $2f_c$ . We now assume that  $\alpha(t)$  and  $\phi(t)$  are affected by a synthetically generated noise with components  $n_\alpha(t)$  and  $n_\phi(t)$ , respectively, as it follows:

$$\begin{aligned} \alpha(t) &= \alpha'(t) + n_\alpha(t), \\ \phi(t) &= \phi'(t) + n_\phi(t), \end{aligned} \quad (4)$$

where  $\alpha'(t)$  and  $\phi'(t)$  represent the actual amplitude and phase components of the baseband signal, respectively. We recall that  $Q(t) = 0$ , when BPSK is considered. Under ideal conditions, Eq. 4 can be rewritten as:

$$\begin{aligned} \alpha(t) &= 1 + \varepsilon_\alpha(t) + n_\alpha(t), \\ \phi(t) &= \{0, \pi\} + \varepsilon_\phi(t) + n_\phi(t), \end{aligned} \quad (5)$$

where we considered the amplitude component  $\alpha'(t) = 1 + \varepsilon_\alpha(t)$ , i.e., a phasor (unitary amplitude) affected by the fingerprint  $\varepsilon_\alpha(t)$  and phase  $\phi'(t) = \{0, \pi\} + \varepsilon_\phi(t)$ , taking on the values either 0 or  $\pi$  as a function of the transmitted bit, while  $\varepsilon_\phi(t)$  is the phase component.

We observe that the amplitude  $n_\alpha(t)$  and phase  $n_\phi(t)$  of the injected noise directly affect the components of the fingerprint, i.e.,  $\varepsilon_\alpha(t)$  and  $\varepsilon_\phi(t)$ . Therefore, the transmitter could hide such components by synthetically injecting noise into the baseband signal. Finally, we highlight that our analysis does not consider any noise coming from the channel, as well as multipath. We prove the reliability of our solution in the later sections of this paper, using real wireless measurements.

As a toy example, consider Fig. 2, where we compare (i) the position of the IQ samples for the ideal BPSK modulation scheme (black crosses), (ii) an actual clear signal  $r(t)$  (green area), and finally, (iii) the noise-obfuscated signal (red area), where the original signal  $r(t)$  has been subjected to the noise components  $n_\alpha(t)$  and  $n_\phi(t)$ . We highlight that the figure is the result of real communication in a wired link, where we applied a Gaussian noise of standard deviation 0.05 simultaneously on the real and imaginary parts of the signal ( $10^5$  IQ samples). In the remainder of this work, we show that such noise intensity is enough to remove the radio fingerprint of the transmitter while negligibly affecting the quality of the signal, i.e., the Signal to Noise Ratio (SNR).

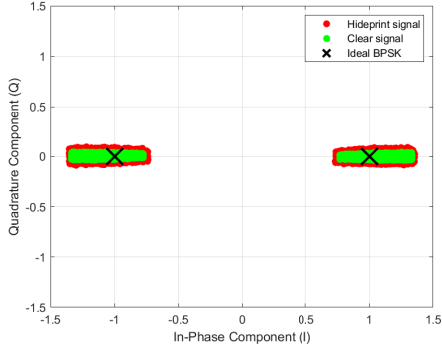


Figure 2: A toy example of our HidePrint solution: the device fingerprint is removed from the clear signal (green area) by adding random noise, thus obtaining the signal dispersed in the red area (signal reshaped by HidePrint). The quality of the received signal remains almost the same.

## 5 Measurement setup

**Software and hardware setup.** Our measurement setup is constituted by a set of Software Defined Radios (SDRs), where the receiver is always an Ettus USRP X410 [31], and we considered a pool of ten (10) transmitters being the USRP B200-mini-i [32], as shown in Fig. 3. We consider a general-purpose laptop running Ubuntu 24.04 LTS running GnuRadio 3.10 (with Python 3.12) and the related flowcharts to control the receiver and each of the transmitters (one per time).

The flowchart for the transmitter (USRP B200-mini-i) involves a standard BPSK modulation scheme, where a repeating sequence of bytes spanning between 0 and 255 is generated considering the block *Vector Source*. The sequence is processed and converted to a stream of bits and, finally, to a stream of complex numbers where the noise ( $n_\alpha(t), n_\phi(t)$ ) (recall Sect. 4) is added before the *Root Raised Cosine Filter*. Finally, our transmitter chain features a *USRP Sink* block used to transmit the signal. The RRC filter performs an upsampling of 4 samples per symbol, i.e., from a symbol rate of 250K IQ symbols per second to  $10^6$  samples per second. All measurements considered in this work assume a carrier frequency  $f_c = 900\text{MHz}$  and a normalized transmitter power of 0.7.

The flowchart for the receiver (ran on the USRP X410) involves a *USRP Source* block with sample rate  $10^6$  (same as the transmitter, according to the modified Nyquist theorem for complex signals [33]), carrier frequency  $f_c = 900\text{MHz}$ , and normalized transmitter gain of 0.7, followed by a *Costas Loop* block, an adaptive gain control *AGC* block, a *Root Raised Cosine Filter* downsampling from 1M sample per second to 512k samples per seconds, and finally, a *Symbol Sync* block implementing the Gardner algorithm for the time error detector and a polyphase filter bank as the interpolating resampler, downsampling the stream from 512K to (the original) 256K samples (symbols) per seconds.

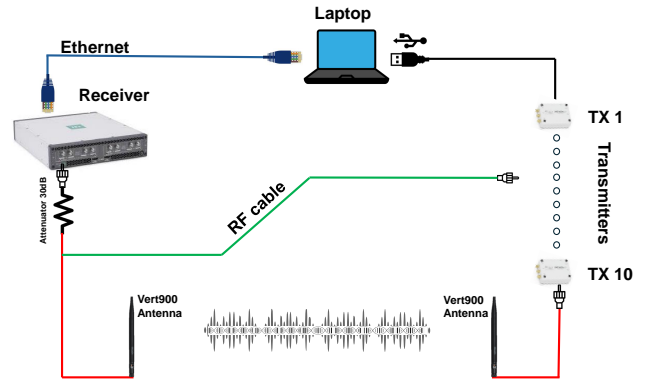


Figure 3: Our measurement setup: 10 transmitters (USRP B200-mini-i) are connected (one per time) to the receiver (USRP X410). We collect data either via an Ethernet cable (USRP X410) or with a USB connection (USRP B200-mini-i). We consider two scenarios: a wired connection between the transmitter and the receiver (green) and a wireless link, where we deployed two Vert900 antennas (red). For both the cases, we considered an attenuator of 30dB.

We stress that the flowcharts considered at both the transmitter and the receiver are designed to reflect as much as possible the standard modulation and demodulation chains implemented in the vast majority of the commercial off-the-shelf transmitters and receivers. In fact, our flowcharts do not expose (or hide) features that might help or prevent the RFF process. As an example, the usage of the *Costas Loop* block—a standard component in any receiver—allows the recovery of the carrier and the synchronization between the clocks between the receiver and the transmitter, but unfortunately, it prevents (non-standard) solutions, like [23], which exploit CFO to perform radio fingerprinting.

**Communication link.** In this work, we consider two types of communication links, i.e., a wired link constituted by an RF cable and a wireless link, where the signal is transmitted and received by using two Vert900 antennas (as per Fig. 3). For both communication links, we consider a signal attenuator of 30dB between the transmitter and the receiver.

The choice of both wired and wireless links aims to understand the impact of wireless channel propagation and multipath fading on the anonymization process. In fact, as introduced in Sect. 4, multipath fading represents another source of noise that potentially helps to prevent the identification of the transmitter at the receiver side.

**Dataset collection.** We collected two datasets of measurements for a total of approximately 167 GB of data, available at [34]. The dataset collected from the wired link ( $\approx 134\text{GB}$ ) is constituted by 240 measurements, i.e., the result of 10 transmitters, 4 types of noise (no noise, Gaussian, Impulse, Laplacian, and Uniform), and 6 noise levels. In contrast, the dataset collected from the wireless link ( $\approx 33\text{GB}$ ) is constituted by 60 measures, i.e., the result of 10 transmitters, 1 types of noise

(Gaussian), and 6 noise levels. Each measurement lasts for 300 seconds, thus providing 750M of IQ samples (recall that the considered symbol rate was 250k symbols per second).

## 6 Device fingerprinting

A critical task in the RFF technique is to mitigate the impact of multipath fading in the fingerprinting process (either during training or testing). As discussed in Sec. 2, several techniques have been proposed during the years, including preprocessing of the IQ samples, adaptation of (only) the first layers of the neural network, up to designing from scratch neural networks able to handle IQ samples. Training and testing (directly) on IQ samples require adapting the neural network (at least for the initial layers) and an ad-hoc preprocessing technique to mitigate the impact of the multipath fading. Recent contributions, e.g., [2, 8, 9, 16, 26–29], show the effectiveness of an orthogonal technique that involves preprocessing IQ samples into images and then using state-of-the-art DL techniques to discriminate and classify images. The root idea consists of generating images from IQ samples while mitigating the impact of the noise by averaging the spatial position of the IQ samples in the IQ plane. As CNNs are a well-known class of DL neural network specifically designed to classify images, image-based RFF techniques use CNNs to discriminate images generated from samples of a specific transmitter, thus performing device fingerprinting. In the following, we recall the most important details associated with the considered methodologies and procedures while pointing the reader to relevant literature for more detailed information.

**Data pre-processing.** Our reference input is a matrix of 2 columns (In-phase and Quadrature components) and 750M of rows, one row for each IQ sample. As depicted in Fig. 2, the vast majority of the IQ plane is not used, and therefore we split the IQ plane into two parts (the positive and the negative In-phase components) and then cut out the 0.005 and 0.0095 quantiles of each axis. Considering the reference value of  $10^5$  IQ samples per image (chunks extracted from the measurement), such a strategy involves removing a total of 2,000 samples per chunk, allowing us to center the image on each cloud of IQ samples while removing outliers, as depicted in Fig. 4(a). The subsequent step consists of computing the bi-variate histogram on the data from Fig. 4(a), as depicted in Fig. 4(b). The number of bins of the bi-variate histogram is defined according to the size (width, height) of the images to be generated, and in turn, according to the input layer of the CNN. As discussed in the following, we consider the CNN *ResNet-18*, already implemented in Matlab2023b, thus setting the image size to 224-by-224 pixels. Figure 4(b) wraps up on the performed computations: the bi-variate histogram counts the IQ samples per bin (i.e., the density), and such value is considered as the value of the pixel in the generated image (lower part of Figure 4(b)). The number of IQ samples considered per image ( $10^5$ ) should be carefully evaluated. Indeed,

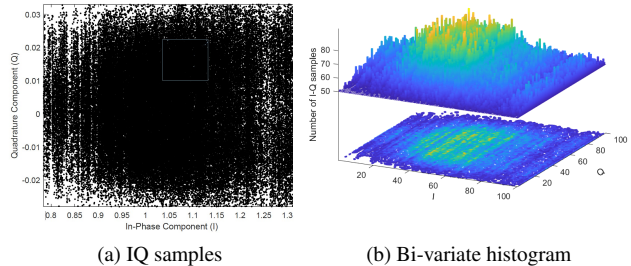


Figure 4: We split the data collected (IQ samples) into chunks of  $10^5$  samples and organized them in one only cloud, i.e., the left cloud of the BPSK modulation is mirrored on the right side. We then compute a bi-variate histogram and consider the output as an image, ready to be processed by a DL algorithm.

a high number of IQ samples per image might generate too many tiles of the bi-variate histogram characterized by values bigger than 255, which is a non-consistent pixel value, thus leading to significant information loss. We carefully estimated the value of the number of IQ samples per image, i.e.,  $10^5$ , with empirical testing and in accordance with [8, 9].

**Deep Learning.** We consider two DL architectures, i.e., CNN and AE, as a function of the attack performed by the adversary (recall Sect. 3). When considering the adversary  $\mathcal{A}_1$ , we assume the adversary targets a finite pool of devices and has already trained a model on the full set. Each device in the pool is willing to keep its anonymity at maximum ( $k$ -anonymity, as per the definition in [35]), i.e., accuracy equal to 0.1, with  $k = 10$  devices in the pool. When considering  $\mathcal{A}_2$ , we consider a targeted attack, i.e., the adversary trains his model on a dataset coming from a specific device, and subsequently, he wants to detect the presence of such device in the radio spectrum. This problem can be addressed as a one-class classification problem, where the samples from the test set are detected as either *legitimate*, if they are recognized to be coming from the target device, or *anomaly*, if they are coming from any other device.

Our reference CNN *ResNet-18* is already implemented in Matlab R2023b and pre-trained on ImageNet [36], in accordance with the *Transfer Learning* design principle. The main objective of this work is not to find the best configuration for the RFF task, which has been addressed in previous work [8]. We choose *ResNet-18* as it represents a good trade-off between accuracy and training time. Moreover, *ResNet-18* cannot be used as is: its last layer requires adaptation to the number of classes (transmitters) in our problem, i.e., 10. Finally, we partially retrained the network by considering a stop criterion according to which the training is interrupted when the accuracy during the validation process achieves a variance across the last 5 iterations less than 0.5.

Our reference *autoencoder* is characterized by 64 neurons in the hidden layer, an encoder transfer function implemented

with the logistic sigmoid function, a decoder transfer function implemented with a linear transfer function, a sparsity regularization coefficient of 0.5, and finally, a  $L_2$  weight regularizer coefficient being equal to 0.01.

While CNNs perform a prediction (class) for each provided image, the autoencoder outputs a reconstruction of the input. In fact, the autoencoder is constituted by an encoder and a decoder. During the training phase, the encoder learns a set of features (latent representation) and these features are used by the decoder to reconstruct the input. This makes the autoencoder applicable in scenarios where a prediction of inputs not previously seen is requested. Given the structure of the autoencoders, a fundamental metric is represented by the reconstruction error since it represents how the reconstructed output is “far away” from the input when reconstructed with the input’s features. In the remainder of this work, we will use the Mean Square Error (MSE) to assess if the image (and the associated IQ samples) belongs to the purported transmitter. An image with  $MSE < \tau$  is predicted to be generated from the target transmitter, while an image with  $MSE > \tau$  is predicted to be generated from another transmitter. For computing  $\tau$ , we adopt Eq. 6, as proposed by the authors in [37].

$$\tau = E(MSE_{train}) + 3.5 \cdot \sigma(MSE_{train}), \quad (6)$$

where  $E(\circ)$  and  $\sigma(\circ)$  represent the mean and the standard deviation, respectively, of the MSE obtained during the validation process.

## 7 Results

In this section, we present the results of our analysis related to two models of adversaries, i.e.,  $\mathcal{A}_1$  and  $\mathcal{A}_2$  (recall Sect 3), while considering increasing prior knowledge. Indeed, we can make two different assumptions on the background knowledge of the adversary, independently of the model. We can assume that the adversary was able to train a model either on noise-free samples or on a combination of noise-free and noisy samples (all samples).

### 7.1 Wired Link - Adversary $\mathcal{A}_1$

**Training on noise-free samples.** We first consider the measurements acquired using the wired communication link and focus on training the *ResNet-18* CNN with noise-free data and testing on any noise level. As previously introduced in Sect. 5, for each device, we collected five different noise levels, i.e., standard deviation  $\sigma = \{0, 0.01, 0.02, 0.03, 0.04, 0.05\}$ , considering five different noise models, i.e., noise-free, Gaussian, Impulse, Laplacian, and Uniform. Therefore, we considered 10 classes (one for each transmitter) and trained a model using the 10 available measurements with noise levels equal to zero. Subsequently, we tested our model considering all combinations of transmitter and noise levels (greater than zero). Figure 5 shows the results of our analysis. In particular, the upper

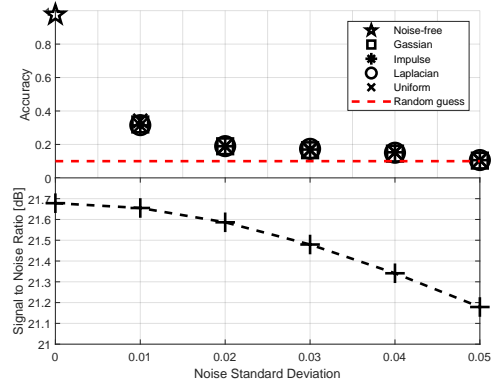


Figure 5: Adversary  $\mathcal{A}_1$  and training on no-noise samples. The adversary trains a model with 10 classes (one for each transmitter) on measurements with no noise and then is challenged to identify the transmitter by considering measurements with noise strictly greater than zero.

part of Fig. 5 depicts the accuracy of the classifier as a function of the noise level ( $\sigma$ ) while considering all the noise types provided by the GnuRadio block *Noise Source*. We observe that the classification accuracy is not affected by the noise type, since they all exhibit the same behavior. In contrast, the accuracy is strongly affected by the noise variance  $\sigma$ , and that  $\sigma \approx 0.02$  is enough to achieve the random guess (accuracy equal to 0.1). In the bottom part of Fig. 5, we considered the SNR as a function of the noise level introduced by the transmitter. We would like to highlight that a variation in the SNR of about 0.1dB is enough to achieve anonymity, thus proving that the quality of the link is negligibly affected by the injection of noise. For the sake of completeness, we recall Fig. 2, which has been generated by considering  $10^5$  samples from the noise-free configuration and  $10^5$  samples from the configuration combining Gaussian noise and  $\sigma = 0.05$ . Finally, we consider the t-Distributed Stochastic Neighbor Embedding (t-SNE) analysis associated with two cases, i.e., noise-free and  $\sigma = 0.02$ , as shown in Fig. 6. The t-SNE analysis performs a dimensionality reduction, i.e., from 10 activations extracted from the last layer of the *ResNet-18* network to a two-dimensional space that can be represented in a Cartesian plane. As can be seen from Fig. 6(a), noise-free values are very well disjoint, and clustering makes it possible to assign each point (image) to the related class. This is not possible in the scenario of Fig. 6(b), where  $\sigma = 0.02$  leads the images coming from the 10 different classes to overlap.

**Training on all samples.** We also consider the scenario where the adversary trains the *ResNet-18* CNN on all the (10) transmitters in the pool and noise levels while considering only the Gaussian noise model—recall from Fig. 5 that different types of noise have the same impact on the fingerprint. To achieve this, we consider the whole dataset and split it into three disjoint chunks, i.e., 60%, 20%, and 20%, for training, validation, and testing, respectively. This adversary configu-

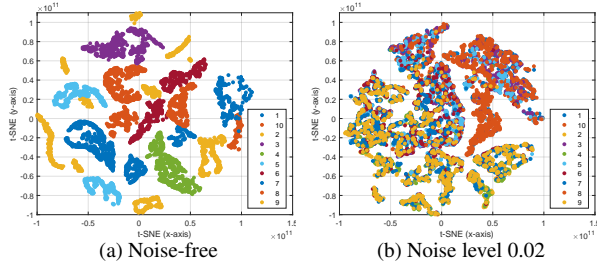


Figure 6: t-SNE analysis for two reference cases: noise-free and  $\sigma = 0.02$ . Classification is possible for the noise-free scenario, but adding noise makes the transmitters virtually indistinguishable.

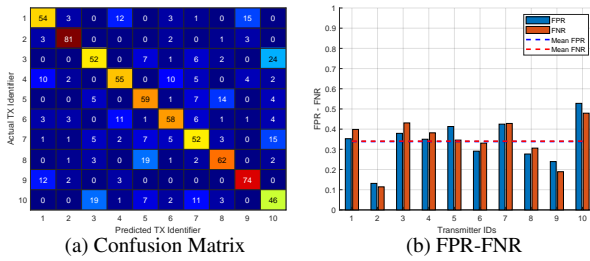


Figure 7: Adversary  $\mathcal{A}_1$  and training on all noise levels. The adversary trains a model with 10 classes (one for each transmitter) on measurements with all the noise levels spanning between 0 and 0.05, and then it is challenged to identify the transmitter by considering random samples taken from random measurements with noise strictly greater than zero.

ration is the most powerful considered in this work. Indeed, as the most favorable condition for the adversary, we assume that the adversary is able to collect (and label) samples from all the transmitters with all the noise levels. Figure 7(a) shows the confusion matrix associated with the actual and predicted transmitters. We observe that, with such knowledge,  $\mathcal{A}_1$  significantly increases its chances of detecting the presence of a transmitter of the pool in the radio spectrum (the average accuracy is about 0.66). Nevertheless, our solution still hides the identity of the transmitters, as depicted in Figure 7(b). Indeed, the average False Positive Ratio (FPR) and False Negative Ratio (FNR), computed on all the transmitters, are similar and equal to 0.35 (dashed red and blue line in Fig. 7(b)). A significant number of transmitters (6 out of 10) are above the average, meaning that when the classifier predicts a specific transmitter, the probability of an error is higher than 0.35. We stress that this value has been obtained by giving to the adversary all the possible knowledge available in the system.

## 7.2 Wired Link - Adversary $\mathcal{A}_2$

**Training on noise-free samples.** We still consider the measurements acquired using the wired link and consider the case of training on noise-free samples for a specific device (only), in line with the adversary model  $\mathcal{A}_2$ . Then, we tested on all the available transmitter configurations, i.e., noise-free and with Gaussian noise with standard deviation  $\sigma = \{0, 0.01, 0.02, 0.03, 0.04, 0.05\}$ . We highlight that we did consider only one noise model (Gaussian) in this case since the noise pattern does not affect the accuracy of the classification process (recall Sec. 7.1 and Fig. 5). Figure 8 shows the results of our analysis in terms of MSE as a function of the transmitter identifier (ID) used for training. Each bar represents the quantiles 5, 50, and 95 associated with the MSE computed on the images generated from the IQ samples. We highlight the comparisons we have made considering four colors: (i) the comparison of the reference set, i.e., two disjoint datasets (60% and 40%) taken from each transmitter ID (red color), one used for training and another one used for testing, respectively; (ii) the comparison of the reference transmitter ID and any other transmitter ID in the pool while considering noise-free samples (blue color), (iii) the comparison of each transmitter ID with the same ID but considering the measurements with the Gaussian noise (green color), and finally, (iv) the comparison of the reference transmitter ID with any other transmitters but considering the measurements with the noise (black color). The red bars in Fig. 8 serve as the reference values. We selected 10 noise-free measurements from each transmitter and then split the generated images into two datasets (60% and 40%) for training and testing, respectively. This setup provides the MSE reference values to be compared with the images coming from other configurations. When comparing the red and blue bars (different transmitter IDs and noise-free measurements), we do not see any (major) overlap that proves that transmitters can be distinguished in a noise-free environment. The minor overlap between the transmitters 2 and 9 will be investigated later on. An orthogonal analysis involves the performance estimation of our solution by comparing the noise-free measurements (red bars) with the ones affected by HidePrint (green bars), where we injected Gaussian noise with different standard deviations. Note that the noise significantly affects the MSE, and in particular, it makes blue bars overlap with the green ones, i.e., the reference transmitter becomes indistinguishable from the others when adding noise to the transmitted signal. Finally, the black error bars consider the measurements with noise from all the transmitters. Note that the noise makes all the measurement configurations overlap, thus achieving indistinguishability between the reference transmitter and the others in the pool.

We now quantify the accuracy that can be achieved considering the attack deployed by adversary  $\mathcal{A}_2$ . For each transmitter, we define a decision threshold according to Eq. 6



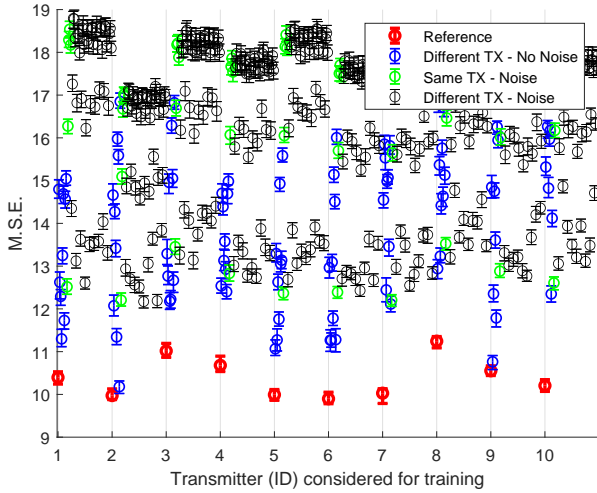


Figure 8: Adversary  $\mathcal{A}_2$  and training on noise-free samples. The adversary trains 10 different models, one for each transmitter considering only the noise-free samples. Red bars represent the test results performed on the same measurements considered for training (considering a split ratio of 80/20). Subsequently, the adversary challenges the trained model with the remainder of the measurement in the dataset: (i) noise-free samples from different transmitters (blue bars), (ii) noisy samples from the same transmitter considered for the training (green bars), and finally, (iii) noisy samples from different transmitters (black bars).

defined earlier. Figure 9 shows the results of our analysis while comparing noise-free signals (green shaded areas) with the remainder of our dataset (red shaded areas). We highlight in blue the thresholds computed for each transmitter. Our analysis shows that the fingerprint (completely) changes when noise is added to the transmitted signal. Indeed, the false positive ratio, i.e., samples from noise-free measurements leading to MSE values larger than the threshold values, is zero, independently of the considered transmitter. Moreover, the false negative ratio, i.e., samples taken from any other measures, is always zero except for two cases, which are about 0.01. This is the case of the transmitters 2 and 9, which have a similar fingerprint (recall Fig. 8). Finally, recalling Fig. 8, we observe that different configurations (noise-free and noisy) eventually collapse in the same range (red shaded areas in Fig. 9), thus making the detection of each of them challenging. For example, an adversary might be able to collect noisy samples with a specific noise level, then train a model, and finally accept the challenge of detecting such a pattern in the radio spectrum. This is unlikely, since all comparisons fall in the region with MSE values between 11 and 19, and therefore, the adversary would experience a high number of misclassifications independently of the chosen configuration.

**Training on all samples.** In the following, we consider

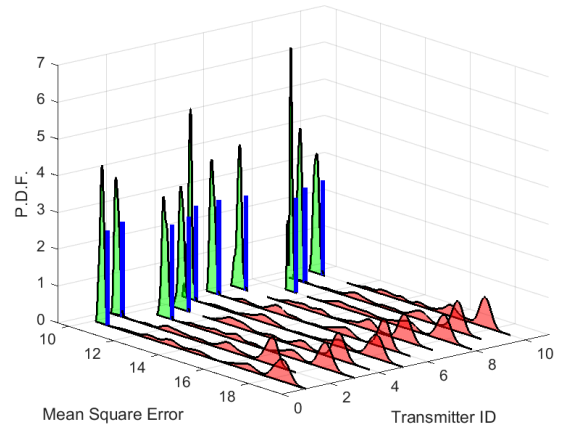


Figure 9: Comparison between MSE values when training on noise-free samples (green curves) and testing on the remainder of the dataset (red curves). We highlight with a blue line the thresholds computed according to Eq. 6. The overlap between the two sets of distributions (red and blue) is negligible for all the transmitters. The autoencoder is successful in distinguishing the transmitters.

the case of adversary  $\mathcal{A}_2$  owning a model trained on both noise-free and noisy samples. Indeed, the adversary has been exposed to the full dataset (noise-free and noisy samples) associated with each device considered in our test. As for the previous case, we considered the Gaussian noise with standard deviation  $\sigma = \{0, 0.01, 0.02, 0.03, 0.04, 0.05\}$ . Figure 10 shows the results of our analysis, where we perform a targeted attack (adversary  $\mathcal{A}_2$ ) on each device of the pool (transmitter IDs). We report, for each of them, the MSE associated with the test set from the selected transmitter ID (green shaded area) and the MSE associated with the other measurements (other transmitters with any noise level). The probability distribution functions overlap for all the transmitter IDs. When considering the threshold defined by Eq. 6 (blue lines in Fig. 10), we obtain an average false negative ratio of about 0.66, confirming that the autoencoder fails to detect the presence of a specific transmitter in the radio spectrum when the training is performed on all the available samples (noise-free and noisy). Such a finding is confirmed by the empirical intuition that a model trained on all the samples cannot differentiate a specific transmitter from the pool since the (injected) noise makes the fingerprint of all the transmitters very similar to each other.

### 7.3 Wireless Link

Our wireless scenario involves the same setup and configuration as the wired one (recall Fig. 3). The transmitters and the receiver have been placed a few meters far away in an office during working time, i.e., with people moving around

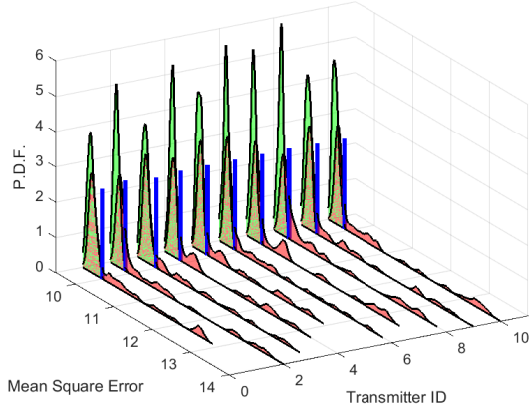


Figure 10: MSE values when training on any samples (green curves) and testing on the remainder of the dataset (red curves). We highlight with a blue line the thresholds computed according to Eq. 6. The overlap between the two sets of distributions (red and blue) is not negligible for all the transmitters (0.66 on average), and thus, the autoencoder fails to distinguish the transmitters.

in close proximity to the transmitter-receiver link, generating multipath. We consider the same data collection procedure as that described for Fig. 5, i.e., Gaussian noise type, CNN *ResNet-18*, and  $10^5$  samples per image. Figure 11 (top) shows the accuracy of *ResNet-18* as a function of the noise standard deviation  $\sigma$ . When  $\sigma = 0$  (noise-free), the accuracy is approximately 0.96, while dropping to 0.16 when  $\sigma = 0.02$ . It is worth noting that an accuracy value of 0.1 is equivalent to a random guess. The SNR is consistent with the one experienced when using the cable: we kept the attenuation to 30dB and the distance between the transmitter and the receiver was only a few meters. Moreover, we observe the existence of a transient region in the range  $]0, 0.02]$  where the accuracy is affected by the combination of different effects, i.e., the fingerprint of the device and the fingerprint of the noise introduced by the channel [26, 27]. The measurements involving the RF cable are not affected by external factors (multipath), and therefore, the fingerprint of the device is the principal component of the received signal. In contrast, when transmitting over the wireless channel, the channel impulse response varies over time depending on the communication link. Therefore, the DL model is likely to experience either consistent or different channel states (channel fingerprint). The final result, as observed by other contributions [8, 26, 27], is that RFF is affected by both the device and the channel fingerprint. The accuracy for  $\sigma = 0.01$  in Fig. 11 (top), being equal to 0.56, is higher than the one in Fig. 5 (top), being equal to 0.25, and it can be explained considering the impact of the channel fingerprint in the overall RFF process: the fingerprint of the wireless channel has a higher impact than the one in the cable. Indeed, the measurements taken considering different transmitters have the same cable with the same channel fingerprint, while

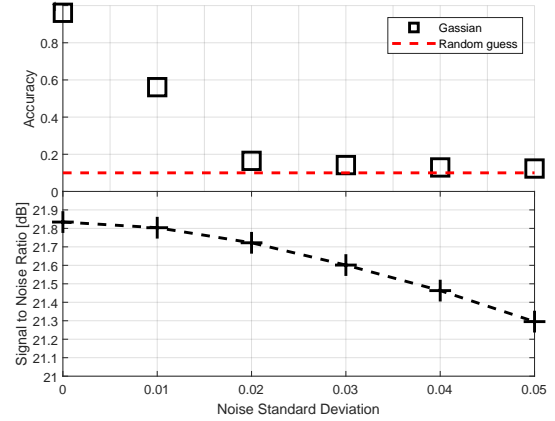


Figure 11: Adversary  $\mathcal{A}_1$  training on noise-free samples from a wireless link. The adversary trains a model with 10 classes (one for each transmitter) on measurements with noise-free samples and then has to identify the transmitter(s) by considering measurements with noise strictly greater than zero.

this is not happening in the radio scenario, where different transmitters might be affected by a (slightly) different radio channel, which helps the classification. Finally, we observe that a noise standard deviation of 0.02 (and higher) can fully anonymize the transmitter independently of the considered measurement scenario. Moreover, the drop associated with the SNR (0.1dB) necessary to remove the fingerprint is consistent with the one experienced using the cable.

We now consider adversary  $\mathcal{A}_2$ , i.e., a targeted attack against a specific transmitter in our pool of 10. We trained an autoencoder on wireless measurements taken from a specific device while setting the noise level  $\sigma$  and tested it on the remainder of the measurements collected from the other transmitters in the pool given the same  $\sigma$ . In fact, we assume  $\mathcal{A}_2$  is capable of training from any type of measurement (noise-free and noisy) and then test it in the wild by collecting samples from the radio spectrum. Figure 12 shows the results of our analysis, where we consider the average Receiver Operating Characteristic (ROC) curves calculated considering the mean value over the 10 transmitters when varying  $\sigma \in \{0, 0.01, 0.02, 0.03, 0.04, 0.05\}$ . Our results confirm our previous findings. First, we observe that the performance of the autoencoder in a noise-free environment (solid blue line in Fig. 12)) is characterized by an FPR and TPR of 0.21 and 0.78, respectively, when considering the point in the ROC curve that offers the best trade-off between sensitivity and specificity, under the assumption that both types of classification errors (TPR and FPR) cost the same—the overall accuracy is equal to 0.81. Moreover, a Gaussian noise with standard deviation  $\sigma = 0.01$  is not enough to de-anonymize the transmitter. Indeed, the solid red line in Fig. 12, representing the ROC curve for  $\sigma = 0.01$ , is characterized by FPR and TPR equal to about 0.27 and 0.7, respectively—the overall accuracy is equal to 0.73. Similarly to the previous case ( $\mathcal{A}_1$ ),  $\sigma = 0.02$

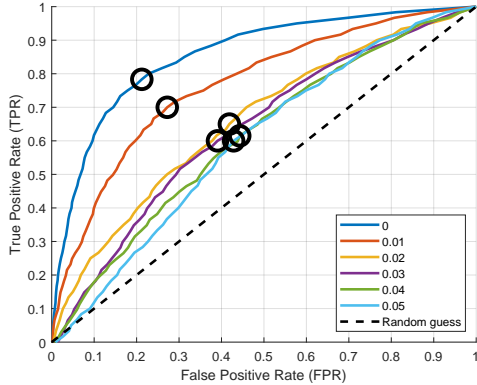


Figure 12: Adversary  $\mathcal{A}_2$ . We trained an autoencoder on measurements taken from a target device and tested against the others in the pool while keeping the same noise level  $\sigma \in \{0, 0.01, 0.02, 0.03, 0.04, 0.05\}$  in an actual wireless link.

allows us to achieve a much better anonymization level, i.e., TPR and FPR values equal to 0.27 and 0.7, respectively, with an overall accuracy equal to 0.64.

## 8 Comparison with other RFF solutions

The RFF methodology used in the previous section to validate HidePrint involves the pre-processing of IQ samples into images, as described in Sect. 6. This strategy has been proven to be effective in mitigating the impact of noise on the RFF process [8]. To provide further insights and show that HidePrint is effective also considering other RFF approaches, in this section, we test our anonymization solution against a different approach considered in the literature, i.e., the use of (raw) IQ samples to train and test a CNN, as considered by [15], [13], and [14]. In order to provide a fair comparison among RFF approaches, we consider the *ResNet-18* network and re-adapt it to accept as input chunks of  $10^4$  IQ samples, so to generate a classification for our pool of 10 (ten) transmitters. The size of the chunk has been evaluated as a trade-off between computation overhead and performance.

We consider the dataset collected in the wireless scenario, training on noise-free samples and then testing on increasing values of  $\sigma$  while considering only the Gaussian noise. Figure 13 shows the results of our analysis. We observe that even with the smallest noise level ( $\sigma = 0.01$ ), the accuracy of RFF via raw IQ samples drops to the random guess (0.1). Figure 13 should be compared with Fig. 11, i.e., same scenario but different methodology (with and without IQ samples pre-processing into images). We observe that both techniques have similar classification performance with noise-free samples ( $\sigma = 0$ ), but image pre-processing is confirmed to be more reliable in the presence of noise: when considering  $\sigma = 0.01$ , the accuracy in Fig. 11 (image-based RFF) is higher than the

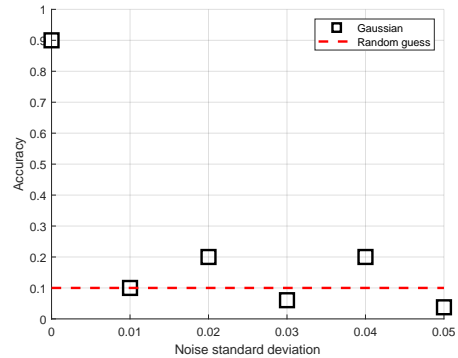


Figure 13: RFF Performance when considering raw IQ samples and different levels ( $\sigma$ ) of Gaussian noise. Standard techniques using raw IQ samples for training and testing are more sensitive to noise injection, thus allowing perfect anonymization even for  $\sigma = 0.01$ .

one in Fig. 13 (raw IQ), although not acceptable for the aim of RFF due to the high value of misprediction ( $> 0.4$ ). For higher values of  $\sigma$ , performance across RFF techniques are the same and confirm the effectiveness of HidePrint.

## 9 Selective Radio Fingerprint Disclosure

The results shown in Sect. 7 show that the adversary (either  $\mathcal{A}_1$  or  $\mathcal{A}_2$ ) does not have any advantage in adding additional noisy samples to the training process to increase the accuracy during the testing phase. In such a case, as shown in Fig. 5, the adversary would experience the disappearance of the fingerprint when the transmitters add an increasing level of noise. Nevertheless, in this section, we investigate the possibility of performing *Selective Radio Fingerprint Disclosure*, i.e., allowing a legitimate receiver to be able to execute RFF even when transmitters are adding noise to the signal, thus authenticating the transmitter while avoiding a non-legitimate party (the adversary) from performing the same.

Let us consider a pool of  $N$  devices, each of them being able to select a noise level in a pool of  $M$  levels. Our analysis shows that, under standard conditions, an adversary cannot infer the identity of the transmitter by guessing it from all the available possibilities  $[N \times M]$ . In the following, we show that we can achieve such a property by sharing with a legitimate receiver only the current adopted noise level while keeping it secret from the adversary. In this way, a legitimate receiver can authenticate the transmitter, but the adversary cannot.

We consider that the  $N$  transmitters in the network are loosely time-synchronized with the receiver, and that the time  $t$  is divided into slots of duration  $T$ , i.e.,  $t : [t_0, \dots, t_\infty]$ . During each time slot, a transmitter can perform at most one communication [38], choosing the standard deviation  $\sigma$  of the noise

level ( $n_i$ ) to be added to the signal according to Eq. 7.

$$n_i = H(s_k | t_i) \quad \text{mod } M, \quad (7)$$

where  $H(\circ)$  is a cryptographically secure hash function,  $s_k$  is the seed (secret to the adversary) preloaded on each transmitter with ID  $k$ , and finally,  $n_i$  is the noise level to be used at time slot  $t_i$ . Each transmitter, at each slot  $t_i$ , computes the noise level to be applied to the radio signal according to a pseudo-random sequence that is unknown to the adversary—under the assumption that the transmitter has not been compromised by the adversary, the seed  $s_k$  is secret to the adversary. The legitimate receiver, aware of the seed  $s_k$ , can obtain the noise level adopted by the transmitter in the current time instant. Under this assumption, the legitimate receiver has a knowledge advantage with respect to the adversary, and can use the appropriate RFF model with respect to the one of the adversary—which is the best that can be adopted under the considered assumptions, i.e.,  $\mathcal{A}_1$  considering all samples. Specifically, in the slot  $t_i$ , the receiver can use a model trained on only 10 classes, i.e., one per transmitter, each for a specific noise pattern. Any other (unauthorized) receivers, unaware of the secret  $s_k$ , is unaware of the noise level used by each transmitter, and has to use a model trained only on noise-free samples, which is more prone to misclassification than the one used by the legitimate receiver (see Fig. 11). Although we acknowledge that such a strategy requires the legitimate receiver to pre-train  $\binom{N}{M}$  models (for each transmitter, all possible noise levels), such training can be done offline. As an example, considering the configuration of this work, the receiver should first pre-train  $\binom{10}{6} = 210$  models in the offline phase. During the later detection phase, the receiver can pick the correct model according to the time slot  $t_i$ , using Eq. 7, and finally test the samples collected from the radio spectrum.

To prove the effectiveness of such a solution against the adversary, we perform Monte-Carlo simulations (100 iterations) by considering a receiver aware of the noise levels considered by the pool of the transmitters. Figure 14 shows the results of our analysis. Our test set consists of (on average) 30 images per transmitter, each image being the result of  $10^5$  IQ samples. The average accuracy from Fig. 14(a) exceeds 0.96, while we reported the false positive (FPR) and false negative rates (FNR) in Fig. 14(b). The performance depicted by the configuration in Fig. 14 should be compared with those in Fig. 7, which is based on the logic used by the adversary. The knowledge of the current adopted noise (as available on a legitimate receiver) increases the accuracy from about 0.66 to 0.96, thus giving the legitimate receiver the opportunity to reliably authenticate the transmitter, opposite to any entity in the network (adversary) not being aware of the seeds ( $s_k$ ).

Let  $\delta$  be the knowledge gap between the legitimate receiver and the adversary, and  $p$  be the probability that the legitimate receiver correctly classifies the transmitters. We can express the probability  $p_{\mathcal{A}}$  that the adversary classifies correctly the transmitters as  $p_{\mathcal{A}} = p - \delta$ . Given a sequence  $w$  of consecutive

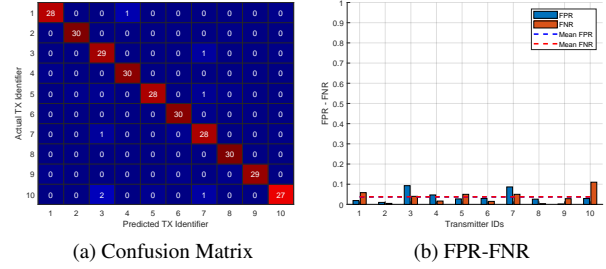


Figure 14: Selective Radio Fingerprint Disclosure. Only the receiver aware of the transmitter seeds  $s_k$  can leverage this information to successfully perform RFF.

observations (images generated from a number of IQ samples), any receiver (including unauthorized ones) can make an educated guess to maximize detection accuracy. Indeed, both the receiver and the adversary can collect  $w$  observations and then apply a majority voting decision on independent observations to maximize their chances of guessing the actual labels to be assigned to the images (transmitting sources)—under the assumption that the seed  $s_k$  is not changed during  $w$ . The probability of getting  $v$  successes in  $w$  independent trials is given by the binomial distribution as per Eq. 8.

$$P(X = v) = \binom{w}{v} p^v (1-p)^{w-v}. \quad (8)$$

The overall outcome is successful if the number of successful RFF classifications  $v$  exceeds  $\lceil \frac{w}{2} \rceil$ . Therefore, the probability that majority voting is successful yields from Eq. 9.

$$P_{succ} = \sum_{v=\lceil \frac{w}{2} \rceil}^w \binom{w}{v} p^v (1-p)^{w-v}. \quad (9)$$

We tested our approach via Monte-Carlo simulations considering  $p = 0.96$  as the probability of successful RFF by the legitimate receiver, in line with the results in Fig. 11. Moreover, we consider an adversary with different knowledge gaps in the range  $\delta = \{0.1, 0.2, 0.3, 0.4, 0.5\}$ . The results of our analysis are shown in Fig. 15, where we highlight with circles markers the probability  $P_{succ}$  of successful RFF by the legitimate receiver, considering majority voting over a growing number of rounds ( $x$ -axis). We use different symbols for various values of knowledge gap  $\delta$ . While increasing the number of rounds  $w$  makes the outcome of the majority voting more decisive, we observe how  $\delta$  gives a significant advantage to the legitimate receiver. Indeed, while  $w = 6$  allows the legitimate receiver to experience an overwhelming probability of correctly guessing the transmitting sources (greater than 0.99), an adversary with a knowledge gap  $\delta = 0.3$ , i.e.,  $p_{\mathcal{A}} = 0.66$ , experiences the same probability of success while adopting the majority voting, i.e.,  $P_{succ} \approx p_{\mathcal{A}}$ .

Finally, we observe that the previous findings can be leveraged by the transmitter to maximize the probability of successful RFF  $P_{succ}$  of the legitimate receiver as opposed to the

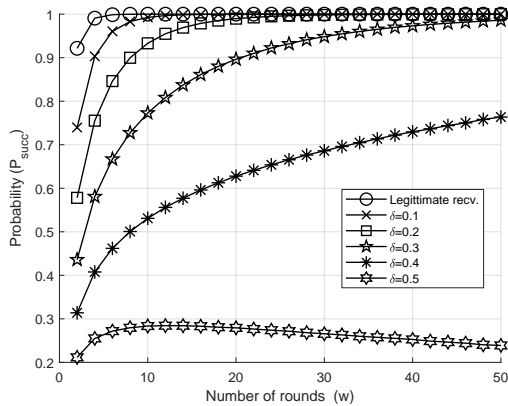


Figure 15: Probability of correct authentication of the transmitter ( $P_{succ}$ ) as a function of the number of rounds (time-slots). A legitimate receiver has an advantage (the knowledge of the seed  $s_k$ ) that can be exploited to maximize its probability of authenticating the transmitter, while an adversary not aware of  $s_k$  has a knowledge gap  $\delta$  which reduces its chances of performing the same task (device authentication).

one of non-authorized receivers, e.g., implementing an update of the seed  $s_k$  every  $w = 3$  rounds.

## 10 Discussion and limitations

This work confirms that RFF can be used to perform de-anonymization attacks at the physical layer against radio devices while proposing an effective and efficient solution to prevent it. The core idea of our proposed solution, HidePrint, relies on injecting noise during the modulation process. The injected noise level should be high enough to hide the fingerprint but enough not to affect the quality of the communication link. Experimental results leveraging both wired and wireless links show that the impact of the noise on the quality of the received signal is less than 0.1 dB while achieving a complete disruption of the fingerprint.

We first collected data from a wired link to estimate the real impact of the noise on the fingerprint, excluding on purpose additional distortion and noise phenomena typical of the wireless channel, such as multipath fading. The ability to identify and track a device is hindered by the injection of noise. This can be achieved by considering any noise pattern and a standard deviation of  $\sigma \geq 0.02$ . We confirmed our findings for wired and wireless links while training on noise-free samples and testing on any other noise level.

We considered two adversary models as a function of the adversary’s capabilities to collect information from the radio devices. We considered different training configurations spanning between noise-free and noisy samples while taking into account either a target device or a pool of devices. All

adversary models considered confirm that the injection of noise prevents the identification and tracking of the device.

Finally, the proposed anonymization technique enables a new form of RFF: *selective device fingerprinting*. A transmitter can control the ability of the receiver to authenticate it (at the physical layer) by resorting to a shared secret. This way, we achieve the implementation of RFF for a controlled subset of receiving entities, i.e., for many but not for all the receivers eavesdropping on the radio spectrum.

**Limitations.** This work is affected by typical limitations of experimental setups. The number of transmitting devices is limited to 10, and all identification attacks have been made against that reference set. We highlight that a pool of 10 devices is aligned with other reference RFF works [8, 15]. We only considered the BPSK modulation scheme, which is consistently used in many wireless technologies, making our results immediately applicable. Although higher-order modulation schemes, e.g., QPSK and 64-QAM, could be more sensitive to noise, we expect such modulation schemes to be well robust to a degradation of the SNR of only 0.1 dB, shown in Fig. 11 as necessary to achieve successful anonymization. We also limited the type of experiments in the wireless scenario by taking into account a static wireless scenario where the transmitter and the receiver are separated by a few meters, while we simulated propagation over larger distances by considering an attenuator of 30dB. The considered scenarios are the ones where RFF exhibits more reliable performance, so we reasonably expect our solution to be robust also in more challenging conditions. Finally, we considered only *ResNet-18* and specific configuration parameters. Although *ResNet-18* is well known to guarantee the best trade-off in terms of accuracy and training time, we plan to test our solution with other CNN while considering different parameters and pre-processing configurations.

## 11 Conclusion and Future Work

We have presented *HidePrint*, a technique to prevent RFF by injecting random noise in the emitted RF signal without affecting communication quality, thus mitigating physical layer attacks aimed at identifying and tracking radio devices. We have tested our solution against state-of-the-art classification techniques, different adversary models, and scenarios. We have proven that the injection of a minimal amount of noise in the transmitted signal does not affect the quality of the link but completely hides the fingerprint from the receiver. Moreover, we have discussed the use of *HidePrint* for selective radio fingerprint disclosure, enabling only a subset of legitimate receivers to perform RFF while excluding other (unauthorized) ones. Future works include testing our solution against different classifiers while considering different deployment scenarios.

## References

- [1] A. Jagannath, J. Jagannath, and P. S. P. V. Kumar, “A comprehensive survey on radio frequency (RF) fingerprinting: Traditional approaches, deep learning, and open challenges,” *Computer Networks*, vol. 219, p. 109455, 2022.
- [2] S. Al-Hazbi, A. Hussain, S. Sciancalepore, G. Oligeri, and P. Papadimitratos, “Radio Frequency Fingerprinting via Deep Learning: Challenges and Opportunities,” in *International Wireless Communications and Mobile Computing (IWCMC)*, 2024, pp. 0824–0829.
- [3] Q. Xu, R. Zheng, W. Saad, and Z. Han, “Device Fingerprinting in Wireless Networks: Challenges and Opportunities,” *IEEE Communications Surveys & Tutorials*, vol. 18, no. 1, pp. 94–104, 2016.
- [4] G. Shen, J. Zhang, A. Marshall, and J. R. Cavallaro, “Towards scalable and channel-robust radio frequency fingerprint identification for LoRa,” *IEEE Transactions on Information Forensics and Security*, vol. 17, pp. 774–787, 2022.
- [5] B. Danev, D. Zanetti, and S. Capkun, “On physical-layer identification of wireless devices,” *ACM Computing Surveys (CSUR)*, vol. 45, no. 1, pp. 1–29, 2012.
- [6] F. Restuccia, S. D’Oro, A. Al-Shawabka, M. Belgiovine, L. Angioloni, S. Ioannidis, K. Chowdhury, and T. Melodia, “DeepRadioID: Real-Time Channel-Resilient Optimization of Deep Learning-based Radio Fingerprinting Algorithms,” in *Proceedings of the Twentieth ACM International Symposium on Mobile Ad Hoc Networking and Computing*, ser. Mobihoc ’19. Association for Computing Machinery, 2019, p. 51–60.
- [7] J. He, S. Huang, S. Chang, F. Wang, B.-Z. Shen, and Z. Feng, “Radio Frequency Fingerprint Identification With Hybrid Time-Varying Distortions,” *IEEE Transactions on Wireless Communications*, vol. 22, no. 10, pp. 6724–6736, 2023.
- [8] S. Alhazbi, S. Sciancalepore, and G. Oligeri, “The Day-After-Tomorrow: On the performance of radio fingerprinting over time,” in *Proc. of the 39th Annual Computer Security Applications Conference*, 2023, pp. 439–450.
- [9] G. Oligeri, S. Sciancalepore, S. Raponi, and R. D. Pietro, “PAST-AI: Physical-layer authentication of satellite transmitters via deep learning,” *IEEE Transactions on Information Forensics and Security*, vol. 18, pp. 274–289, 2023.
- [10] B. Danev, H. Luecken, S. Capkun, and K. El Defrawy, “Attacks on physical-layer identification,” in *Proceedings of the Third ACM Conference on Wireless Network Security*, ser. WiSec ’10, 2010, p. 89–98.
- [11] L. F. Abanto-Leon, A. Bäuml, G. H. Sim, M. Hollick, and A. Asadi, “Stay Connected, Leave no Trace: Enhancing Security and Privacy in WiFi via Obfuscating Radiometric Fingerprints,” *Proceedings of the ACM on Measurement and Analysis of Computing Systems*, vol. 4, no. 3, pp. 1–31, 2020.
- [12] L. Papangelo, M. Pistilli, S. Sciancalepore, G. Oligeri, G. Piro, and G. Boggia, “Adversarial Machine Learning for Image-Based Radio Frequency Fingerprinting: Attacks and Defenses,” *IEEE Communications Magazine*, pp. 1–7, 2024.
- [13] B. Liu, et al., “Robust Adversarial Attacks on Deep Learning Based RF Fingerprint Identification,” *IEEE Wireless Communications Letters*, 2023.
- [14] L. Sun, et al., “Robustness of Deep Learning-Based Specific Emitter Identification under Adversarial Attacks,” *Remote Sensing*, vol. 14, no. 19, p. 4996, 2022.
- [15] Z. Lu, W. Xu, M. Tu, X. Xie, C. Hua, and N. Cheng, “Erasing Radio Frequency Fingerprints via Active Adversarial Perturbation,” 2024. [Online]. Available: <https://arxiv.org/abs/2406.07349>
- [16] M. Irfan, S. Sciancalepore, and G. Oligeri, “Preventing Radio Fingerprinting through Friendly Jamming,” *arXiv preprint arXiv:2407.08311*, 2024.
- [17] D. R. Reising, M. A. Temple, and J. A. Jackson, “Authorized and rogue device discrimination using dimensionally reduced RF-DNA fingerprints,” *IEEE Transactions on Information Forensics and Security*, vol. 10, no. 6, pp. 1180–1192, 2015.
- [18] Z. Zhuang, X. Ji, T. Zhang, J. Zhang, W. Xu, Z. Li, and Y. Liu, “Fbsleuth: Fake base station forensics via radio frequency fingerprinting,” in *Proceedings of the 2018 on Asia Conference on Computer and Communications Security*, 2018, pp. 261–272.
- [19] D. Reising, J. Cancellieri, T. D. Loveless, F. Kandah, and A. Skjellum, “Radio identity verification-based IoT security using RF-DNA fingerprints and SVM,” *IEEE Internet of Things Journal*, vol. 8, no. 10, pp. 8356–8371, 2020.
- [20] A. Al-Shawabka, F. Restuccia, S. D’Oro, T. Jian, B. C. Rendon, N. Soltani, J. Dy, S. Ioannidis, K. Chowdhury, and T. Melodia, “Exposing the fingerprint: Dissecting the impact of the wireless channel on radio fingerprinting,” in *IEEE INFOCOM 2020-IEEE Conference on Computer Communications*. IEEE, 2020, pp. 646–655.

- [21] G. Shen, J. Zhang, A. Marshall, L. Peng, and X. Wang, "Radio frequency fingerprint identification for LoRa using deep learning," *IEEE Journal on Selected Areas in Communications*, vol. 39, no. 8, pp. 2604–2616, 2021.
- [22] A. Elmaghub and B. Hamdaoui, "No Blind Spots: On the Resiliency of Device Fingerprints to Hardware Warm-Up Through Sequential Transfer Learning," in *Proceedings of the 17th ACM Conference on Security and Privacy in Wireless and Mobile Networks*, ser. WiSec '24, 2024, p. 134–144.
- [23] A. Elmaghub and B. Hamdaoui, "Distinguishable iq feature representation for domain-adaptation learning of wifi device fingerprints," *IEEE Transactions on Machine Learning in Communications and Networking*, vol. 2, pp. 1404–1423, 2024.
- [24] X. Gu, W. Wu, A. Song, M. Yang, Z. Ling, and J. Luo, "RF-TESI: Radio Frequency Fingerprint-based Smartphone Identification under Temperature Variation," *ACM Transactions on Sensor Networks*, vol. 20, no. 2, pp. 1–21, 2024.
- [25] M. Irfan, S. Sciancalepore, and G. Oligeri, "On the Reliability of Radio Frequency Fingerprinting," *arXiv preprint arXiv:2408.09179*, 2024.
- [26] A. Sadighian, S. Sciancalepore, and G. Oligeri, "Sat-Print: Satellite link fingerprinting," in *2024 ACM Symposium on Applied Computing (SAC)*, 2024, pp. 177–185.
- [27] A. Sadighian, S. Sciancalepore, and G. Oligeri, "Fade-Print: Satellite spoofing detection via fading fingerprinting," in *2024 IEEE 21th Consumer Communications & Networking Conference (CCNC)*, 2024.
- [28] S. Alhazbi, S. Sciancalepore, and G. Oligeri, "Bloodhound: Early detection and identification of jamming at the phy-layer," in *IEEE Consumer Communications & Networking Conference (CCNC)*, 2023, pp. 1033–1041.
- [29] S. Sciancalepore, F. Kusters, N. K. Abdelhadi, and G. Oligeri, "Jamming Detection in Low-BER Mobile Indoor Scenarios via Deep Learning," *IEEE Internet of Things Journal*, vol. 11, no. 8, pp. 14 682–14 697, 2024.
- [30] T. S. Rappaport, *Wireless communications: principles and practice*. Cambridge University Press, 2024.
- [31] National Instruments, "NI USRP X410 Specification," Data Sheet.
- [32] National Instruments, "NI USRP b200 mini-i Specification," Data Sheet.
- [33] DSP StackExchange, "Bandwidth with complex sampling," <https://dsp.stackexchange.com/questions/36927/bandwidth-with-complex-sampling>, Apr. 2017, (Accessed: 2024-Nov-01).
- [34] G. Oligeri and S. Sciancalepore, "Open Source Data of HidePrint measurements," <https://tinyurl.com/82udhrd8>, accessed: 01-Nov-2024.
- [35] P. Samarati and L. Sweeney, "Protecting privacy when disclosing information: k-anonymity and its enforcement through generalization and suppression," 1998.
- [36] J. Deng, W. Dong, R. Socher, L.-J. Li, K. Li, and L. Fei-Fei, "Imagenet: A large-scale hierarchical image database," in *2009 IEEE conference on computer vision and pattern recognition*. Ieee, 2009, pp. 248–255.
- [37] S. M. Erfani, S. Rajasegarar, S. Karunasekera, and C. Leckie, "High-dimensional and large-scale anomaly detection using a linear one-class SVM with deep learning," *Pattern Recognition*, vol. 58, pp. 121–134, Oct. 2016.
- [38] R. Di Pietro and G. Oligeri, "Enabling broadcast communications in presence of jamming via probabilistic pairing," *Computer Networks*, vol. 116, pp. 33–46, 2017.